

Realizing a Kondo-correlated state with ultracold atoms

Johannes Bauer,¹ Christophe Salomon,² and Eugene Demler¹

¹ *Department of Physics, Harvard University, Cambridge, Massachusetts 02138, USA and*

² *Laboratoire Kastler Brossel, CNRS, UPMC, Ecole Normale Supérieure, 24 rue Lhomond, 75231 Paris, France*

(Dated: January 8, 2022)

We propose a novel realization of Kondo physics with ultracold atomic gases. It is based on a Fermi sea of two different hyperfine states of one atom species forming bound states with a different species, which is spatially confined in a trapping potential. We show that different situations displaying Kondo physics can be realized when Feshbach resonances between the species are tuned by a magnetic field and the trapping frequency is varied. We illustrate that a mixture of ^{40}K and ^{23}Na atoms can be used to generate a Kondo correlated state and that momentum resolved radio frequency spectroscopy can provide unambiguous signatures of the formation of Kondo resonances at the Fermi energy. We discuss how tools of atomic physics can be used to investigate open questions for Kondo physics, such as the extension of the Kondo screening cloud.

PACS numbers: 67.85.Pq,72.10.Fk,72.15.Qm,75.20.Hr

Introduction - Significant advances in quantum optics, such as in cooling, trapping and manipulating ultracold atoms, have lead to the realization of a plethora of exciting many-body phases in a controlled manner [1, 2]. An important drive for this field is that many of these phases and their description in terms of model Hamiltonians are of great interest in condensed matter physics, such that a fruitful interplay of these fields has developed. It has, for instance, been possible to realize superfluid phases both in fermionic and bosonic systems and the transition to a Mott insulating regime [3–8].

An intriguing many-body effect in condensed matter physics is the Kondo effect. It occurs when itinerant fermions interact with magnetic impurities, such as, for instance, a small concentration of Fe in Au. The orbital occupation of the impurity must be such that there is an unscreened spin present, i.e., in the simplest case a localized state occupied by a single electron. The essence of the Kondo effect is then that at low temperature this electron spin forms a many-body bound state with the itinerant electrons and becomes magnetically screened. Crucial for this magnetic screening are second order processes which lead to frequent spin flips. This Kondo-correlated state leads to a distinctive feature in the resistivity (Kondo minimum) and was also observed as enhanced transport in quantum dots [9, 10].

In spite of decades of intense research [11], there remain unresolved questions. For instance, a Kondo screening cloud with a certain spatial extent and characteristic oscillations was predicted [11–14], however, its experimental observation has remained elusive. On increasing the impurity concentration from very few to a full lattice, the Kondo clouds overlap and the localized spins interact with each other via the so-called Ruderman-Kittel-Kasuya-Yoshida (RKKY) coupling, mediated by the itinerant fermions. This generates a competing effect to the Kondo screening and leads to a transition to a magnetically ordered state of the spins. The Kondo lattice prob-

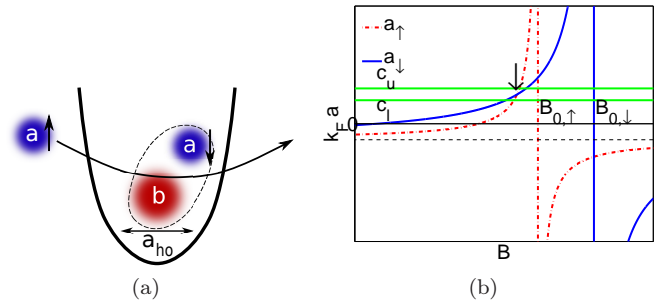


FIG. 1: (Color online) (a) Schematic picture of an atomic bound state of an a species atom with a b species atom in a harmonic trap with oscillator length a_{ho} . (b) Schematic plot of the effective scattering length a_{σ} close to a Feshbach resonance for a case where the $a_{\uparrow} = a_{\downarrow}$ is satisfied within a suitable regime of parameters for Kondo physics given by the boundaries (c_l, c_u) as explained in the text.

lem is of paramount importance for the understanding of heavy fermion systems and quantum criticality [15, 16], however, it is very hard to analyze it theoretically beyond the mean field level. Here, we propose an experimental setup based on ultracold atoms to realize single impurity and lattice Kondo situations. The Kondo scale is shown to be accessible by current experimental techniques.

In the field of ultracold atoms, a lot of progress has recently been made for manipulating mixtures of different species that offer the unique possibility to selectively trap one species and to handle heteronuclear Feshbach resonances producing molecular bound states [17–22]. These developments are important ingredients for our proposal. The main idea is to allow atoms of a Fermi sea to form bound states with a different, spatially confined atom, the impurity [see Fig. 1 (a)]. We consider two species of ultracold atoms with mass m_a, m_b . Species a is fermionic and is prepared in two different hyperfine states labeled by a spin index σ . Species b , which can be a fermion or boson, is subject to a strong harmonic confining potential. The bound states for the hyperfine states cor-

respond to the unscreened spin in the Kondo problem. In order for the Kondo effect to occur the bound states need to obey certain conditions. First, the bound state between the a and b atoms needs to be well occupied, however, the atoms should not be too tightly bound such that second order spin flip processes - important for the Kondo effect - can occur frequently. This implies a certain regime for the effective scattering lengths a_σ bounded by c_u and c_l as shown in Fig. 1 (b). Second, the bound states energies should be very similar, since a difference of their energy will favor a certain polarization of the spin, like a magnetic field, which suppresses the Kondo effect. The bound state energies of atom a with b , $E_{b,\sigma}$, generally depend on the scattering lengths a_σ , $E_{b,\sigma} \simeq -\hbar^2/2m_r a_\sigma^2$, $m_r = m_a m_b / (m_a + m_b)$, and for a general system those will be very different. The challenge is then to find a scheme in which the bound states can be simultaneously tuned to an energy which is roughly equal and in a suitable regime for Kondo physics. As we will show, for certain hyperfine states of a system of ^{40}K and ^{23}Na atoms the effective scattering lengths intersect in this regime when tuned close to Feshbach resonances such that Kondo physics is directly possible. However, for many other systems this fortuitous meeting of the conditions will not occur. In the Supplementary Material (SM) we show that additional resonances of the confining potential can also be employed to tune the system into the Kondo-correlated state [23, 24].

Physical setup and effective model - To formalize these ideas, we first discuss the atomic scattering problem and then relate the parameters to the low energy effective model in Eq. (5), which is directly connected to the Kondo effect. Consider for each component σ the two-particle scattering between species a and b described by a Hamiltonian of the form,

$$H_{\text{scat}} = \frac{p_b^2}{2m_b} + \frac{1}{2}m_b\omega_{\text{ho}}^2 r_b^2 + \frac{p_a^2}{2m_a} + V(\mathbf{r}_a - \mathbf{r}_b), \quad (1)$$

where \mathbf{p}_α , \mathbf{r}_α are momenta and positions of the particles, $V(\mathbf{r})$ is the interspecies potential and ω_{ho} a scale for the harmonic confinement. A corresponding length scale is the harmonic oscillator length $a_{\text{ho}} = \sqrt{\hbar/m_b\omega_{\text{ho}}}$. The low energy form of the effective s-wave scattering amplitude $f_\sigma(k)$ in terms of a_σ and the effective radius $r_{e,\sigma}$ is,

$$f_\sigma(k) = \frac{1}{-\frac{1}{a_\sigma} + r_{e,\sigma}\frac{k^2}{2} - ik}. \quad (2)$$

Without the harmonic confinement ($\omega_{\text{ho}} = 0$) the scattering problem for each σ is characterized by the bare s-wave scattering length $a_{0,\sigma}$. In presence of the harmonic trap the effective parameters a_σ and $r_{e,\sigma}$ can be calculated depending on the bare scattering length $a_{0,\sigma}$ [24, 25]. One finds in the Born approximation,

$$a_\sigma = \frac{m_a}{m_r} a_{0,\sigma}, \quad r_{e,\sigma} = -\frac{m_r}{m_a} \frac{a_{\text{ho}}^2}{a_{0,\sigma}}. \quad (3)$$

To tune the bare scattering lengths $a_{0,\sigma}$ by a magnetic field B , we assume that there is a Feshbach resonance,

$$a_{0,\sigma}(B) = a_{\text{bg}} \left(1 - \frac{\Delta B_{0,\sigma}}{B - B_{0,\sigma}} \right), \quad (4)$$

where a_{bg} is the background scattering length, $\Delta B_{0,\sigma}$ the width and $B_{0,\sigma}$ the position of the resonance.

We describe the low energy physics of the system by an Anderson impurity model (AIM) [26] of the form,

$$H = \sum_{\mathbf{k},\sigma} \varepsilon_{\mathbf{k}} c_{\mathbf{k},\sigma}^\dagger c_{\mathbf{k},\sigma} + \sum_{\sigma} \varepsilon_{b,\sigma} c_{b,\sigma}^\dagger c_{b,\sigma} + U n_{b,\uparrow} n_{b,\downarrow} + \sum_{\mathbf{k},\sigma} V_{\mathbf{k},\sigma} c_{\mathbf{k},\sigma}^\dagger c_{b,\sigma} + \text{h.c.} \quad (5)$$

Here, $c_{\mathbf{k},\sigma}^\dagger$ creates an itinerant fermion with momentum \mathbf{k} and spin projection σ , and $c_{b,\sigma}^\dagger$ a bound state with energy $\varepsilon_{b,\sigma}$. The states are mixed by the hybridization $V_{\mathbf{k},\sigma}$. Three-particle bound states are assumed to be highly unstable due to rapid decay into deep two-body bound states [27, 28]. Under such conditions it has been shown [29] that the system corresponds to $U \rightarrow \infty$, where the occupation of those states is suppressed. Particle loss is inhibited in such situations [29]. The effect of the shallow trapping potential on the atoms with mass m_a is neglected, and hence the dispersion is $\varepsilon_{\mathbf{k}} = \hbar^2 \mathbf{k}^2 / 2m_r$ [56]. We focus on the case of three spatial dimensions, where the corresponding density of states (DOS) per spin is $\rho_0(\varepsilon) = c_3 \sqrt{\varepsilon}$, with $c_3 = V_0 k_F^3 / (4\pi^2 \varepsilon_F^{3/2})$, and $\varepsilon_F = \frac{\hbar^2}{2m_r} (3\pi^2 n)^{2/3}$. Here, $n = N_a / V_0$, where V_0 is the volume of the system and N_a the number of particles of species a .

Relation of AIM parameters to scattering parameters - The scattering amplitude is related to the T -matrix by

$$f_\sigma(\mathbf{k}, \mathbf{k}) = -V_0 \frac{m_r}{2\pi\hbar^2} T_{\mathbf{k},\mathbf{k}}^\sigma. \quad (6)$$

We can express the right hand side in terms of scattering properties of the AIM, $T_{\mathbf{k},\mathbf{k}}^{A,\sigma}(\omega = \varepsilon_{\mathbf{k}})$, and from this determine the model parameters in Eq. (5). The T -matrix of the AIM is given by [11],

$$T_{\mathbf{k},\mathbf{k}'}^{A,\sigma}(\omega) = V_{\mathbf{k},\sigma}^* G_{b,\sigma}(\omega) V_{\mathbf{k}',\sigma}, \quad (7)$$

where $G_{b,\sigma}(\omega)$ is the retarded bound state Green's function, $\eta \rightarrow 0$,

$$G_{b,\sigma}(\omega)^{-1} = \omega + i\eta - \varepsilon_{b,\sigma} - K_\sigma(\omega) - \Sigma_\sigma(\omega). \quad (8)$$

Generally, impurity properties only depend on the integrated hybridization term $K_\sigma(\omega) = \sum_{\mathbf{k}} \frac{|V_{\mathbf{k},\sigma}|^2}{\omega + i\eta - \xi_{\mathbf{k}}}$, where we defined $\xi_{\mathbf{k}} = \varepsilon_{\mathbf{k}} - \mu$.

A full solution of the scattering problem in Eq. (1) yields f_σ [24] such that the AIM parameters can be determined numerically via Eq. (6). Here we take a simplified form, $V_{\mathbf{k},\sigma} = V_\sigma$, which is real and constant for

$\varepsilon_{\mathbf{k}} < \Lambda_{v,\sigma}$ and zero otherwise. This allows us to derive explicit analytical expressions. For generic forms of free states and an s-wave bound state, one sees that the overlap integrals $V_{\mathbf{k},\sigma}$ vanish when the wave length $1/k$ becomes much shorter than the typical extension of the bound state a_σ . From this follows that a reasonable assumption is $\Lambda_{v,\sigma} = \frac{\alpha^2}{(k_F a_\sigma)^2} \varepsilon_F$, with $\alpha \simeq 1$, used in the following. From Eq. (6) we find then for small k with Eq. (2) and Eq. (7) with $\mu \rightarrow 0$,

$$\frac{V_\sigma^2}{\varepsilon_F^2} = \frac{\frac{8\pi}{V_0 k_F^3}}{\frac{2}{\pi} |k_F a_\sigma| - k_F r_{e,\sigma}}, \quad (9)$$

such that $V_\sigma^2 \sim 1/N_a$ and

$$\frac{\varepsilon_{b,\sigma}}{\varepsilon_F} = \frac{V_0 k_F^3}{4\pi} \left(\frac{2}{\pi |k_F a_\sigma|} - \frac{1}{k_F a_\sigma} \right) \frac{V_\sigma^2}{\varepsilon_F^2} = 2 \frac{\frac{2}{\pi |k_F a_\sigma|} - \frac{1}{k_F a_\sigma}}{\frac{2}{\pi} |k_F a_\sigma| - k_F r_{e,\sigma}}. \quad (10)$$

Useful quantities are the hybridization parameter, $\Gamma_\sigma = \pi \rho_0(\varepsilon_F) V_\sigma^2$, which is independent of the volume of the system, and the important ratio

$$\frac{-\varepsilon_{b,\sigma}}{\pi \Gamma_\sigma} = \frac{1}{\pi} \left(\frac{1}{k_F a_\sigma} - \frac{2}{\pi |k_F a_\sigma|} \right), \quad (11)$$

which only depends on $k_F a_\sigma$. We can see how the AIM model parameters depend on a_σ and $r_{e,\sigma}$, for instance, $-\varepsilon_{b,\sigma}$ increases with $1/a_\sigma$ for $a_\sigma > 0$. As discussed, a_σ and $r_{e,\sigma}$ depend on $a_{0,\sigma}$ and thus on the magnetic field B and the trapping frequency ω_{ho} , and this allows to tune the model parameters in Eq. (5). We see that in general both $h = (\varepsilon_{b,\uparrow} - \varepsilon_{b,\downarrow})/2$, which acts as a local magnetic field, and $\Delta\Gamma = (\Gamma_\uparrow - \Gamma_\downarrow)/2$ can be non-zero. For studies of the AIM the latter is unusual, but it has been discussed in situations of quantum dots coupled to partly polarized leads [30–32]. As discussed in the SM, this implies that in general due to second order processes in the hopping an effective local magnetic field h_{eff} is generated. There, also the mapping of the general AIM in Eq. (5) to an anisotropic Kondo model with spin-spin couplings $J_\perp \neq J_z$ and the derivation of the Kondo scale T_K from scaling equations are explained.

Tuning to the Kondo state - We now discuss appropriate parameter regimes to observe the Kondo-correlated state in more detail. These are meant as guidelines and not strict boundaries. The first condition (I) is to have small fluctuations of the occupation of the bound state, which can be expected if $-\varepsilon_{b,\sigma}/(\pi\Gamma_\sigma) > c_1$. A naive estimate is $c_1 \sim 1/2$, however, smaller values, $c_1 \sim 0.25$, also work well as shown later. The second condition (II) is to have the Kondo scale in a regime where it can be observed experimentally, i.e., the experimental temperature $T_{\text{exp}} \sim T_K$. We assume $T_{\text{exp}} = \alpha_T \varepsilon_F$, where $\alpha_T \sim 0.01$ can be achieved. To achieve this the bound state must not lie too deep. More formally, T_K depends exponentially on the Kondo coupling J_z and the

asymmetry $x = J_\perp/J_z < 1$. It follows that J_z must not be too small and the asymmetry should not be too large. These couplings depend on the AIM parameters $\varepsilon_{b,\sigma}, \Gamma_\sigma$ (see SM) and we can obtain a condition of the form $-1/2 \sum_\sigma \varepsilon_{b,\sigma}/(\pi\Gamma_\sigma) < c_2$ with a numerical estimate $c_2 \approx 0.6$. Hence, together with (I) we define an interval for values of $-\varepsilon_{b,\sigma}/(\pi\Gamma_\sigma)$, and with the help of Eq. (11) we can state it as a condition for $k_F a_\sigma$,

$$c_l < k_F a_\sigma < c_u, \quad (12)$$

where $c_l = \frac{\pi-2}{\pi^2 c_2}$, $c_u = \frac{\pi-2}{\pi^2 c_1}$ are lower/upper boundaries [see Fig. 1 (b)]. For $\Delta\Gamma \neq 0$, an effective magnetic field is generated, which suppresses Kondo correlations. It is possible to offset the effective field with a local magnetic field h , and thus, we define a third condition (III), $\Delta\Gamma = \alpha_h h$. For a symmetric DOS, $\alpha_h \simeq 0.2$ was found numerically [31], however, for a general DOS and different cut-offs this may vary (see SM).

To be able to tune to the Kondo-correlated state, it is necessary to have a system, where the Feshbach resonances for $|\uparrow\rangle$ and $|\downarrow\rangle$ with the impurity atom have some overlap. Using the form in Eq. (4) for $a_{0,\sigma}$, $\Delta B_{0,\uparrow}$ and $\Delta B_{0,\downarrow}$ need to have the same sign and $|B_{0,\sigma} + \Delta B_{0,\sigma}| > |B_{0,-\sigma}|$. Given the bare scattering lengths $a_{0,\sigma}$ the effective scattering length including the harmonic potential can be calculated. For simplicity we use the Born approximation in Eq. (3) in the following, which was shown to give reasonably accurate results [24]. Hence, the effective scattering lengths can be tuned close to the Feshbach resonance and it is possible that at the intersection, $a_\uparrow = a_\downarrow$, Eq. (12) is satisfied. This is illustrated in Fig. 1 (b). As $a_{0,\uparrow} = a_{0,\downarrow}$, Eq. (3) implies $r_{e,\uparrow} = r_{e,\downarrow}$, such that $h = \Delta\Gamma = 0$ and automatically conditions (I-III) are satisfied. Note that if $a_\uparrow = a_\downarrow$, but $k_F a_\sigma > c_u$, we can satisfy Eq. (12) by reducing the density n and thus k_F .

Experimental system and probe- For the experimental realization of our proposal we focus on a system of ^{40}K with $|\downarrow\rangle \equiv |9/2, -7/2\rangle$ and $|\uparrow\rangle \equiv |9/2, -5/2\rangle$ hyperfine states and ^{23}Na in the hyperfine state $|1, 1\rangle$. In this system recently molecular states were successfully produced using interspecies Feshbach resonances [20]. For our purpose, the Feshbach resonances with $B_{0,\uparrow} = 106.9\text{G}$, $B_{0,\downarrow} = 108.6\text{G}$, $\Delta B_{0,\uparrow} = -1.8\text{G}$, and $\Delta B_{0,\downarrow} = -6.6\text{G}$ [19] are suitable. The background scattering length is $a_{\text{bg}} = -690a_B$, where the Bohr radius is $a_B = 0.53 \cdot 10^{-10}\text{m}$. In the following we use common values in ultracold gas experiments, $n \sim 10^{18}\text{m}^{-3}$, $k_F^0 = [3\pi^2 n]^{1/3} = 1.6 \cdot 10^{-4}/a_B$. A typical trapping frequency is $\omega_{\text{ho}} \sim 100\text{kHz}$ [1], such that for ^{23}Na we have $a_{\text{ho}} = 3.12 \cdot 10^3 a_B$. One has $a_{0,\uparrow} = a_{0,\downarrow} = -1.82 a_{\text{bg}}$ for

$$B_s = \frac{B_{0,\downarrow} \Delta B_{0,\uparrow} - B_{0,\uparrow} \Delta B_{0,\downarrow}}{\Delta B_{0,\uparrow} - \Delta B_{0,\downarrow}} = 106.26\text{G}. \quad (13)$$

With Eq. (3), this implies $k_F^0 a_\sigma = 0.55$. Employing the numerical renormalization group (NRG) [33, 34], we cal-

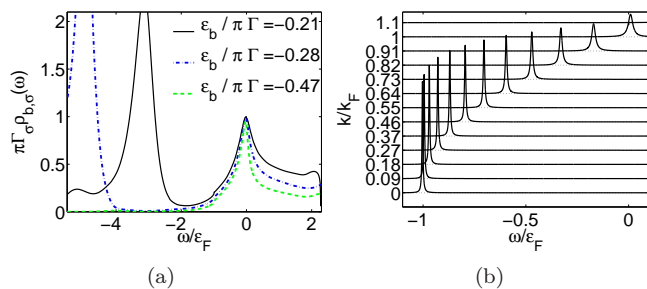


FIG. 2: (Color online) (a) Spectral function $\rho_{b,\sigma}(\omega)$ for different values of $\varepsilon_{b,\sigma}/\pi\Gamma$ obtained for $k_F = 1, 0.75, 0.45k_F^0$. The corresponding values are $k_F a_\sigma = 0.55, 0.41, 0.25$ and the complete set of AIM parameters is given in Table I in the SM. The magnetic field B has been tuned such that $a_\uparrow = a_\downarrow$. (b) Momentum resolved spectral function $\rho_{\mathbf{k},\sigma}(\omega)$ as calculated from Eq. (14) for the case $\varepsilon_b/\pi\Gamma = -0.21$ with n_{imp} as discussed below Eq. (14).

culated the low temperature bound state spectral function, $\rho_{b,\sigma}(\omega)$, for parameters corresponding to the K-Na-system for the situation where $B = B_s$ in Eq. (13) and we vary k_F/k_F^0 , where k_F^0 is as above. The energy scale is set by $\varepsilon_F = 1$, and we measure all energies from ε_F . The numerical values for the AIM parameters are given in Table I in the SM. The result is shown in Fig. 2 (a). The bound state peaks lie between $-8\varepsilon_F$ (not shown) and $-2\varepsilon_F$. Due to interaction effects the peaks are broadened, even though they lie outside the continuum, however, the width might be overestimated in the NRG calculation. At $\omega = 0$ we see a clear peak, the Kondo or Abrikosov-Suhl resonance. We can extract the half width of the Kondo resonance $\Delta_K \sim 0.1\varepsilon_F$, which is indicative of the Kondo scale suitable for experimental observations.

We will now describe experimental signatures to detect the Kondo-correlated state. The retarded Green's function of itinerant states in presence of n_{imp} impurities is given by [11],

$$G_{\mathbf{k},\sigma}(\omega)^{-1} = \omega + i\eta - \xi_{\mathbf{k}} - n_{\text{imp}}V_\sigma^2 G_{b,\sigma}(\omega), \quad (14)$$

and $\rho_{\mathbf{k},\sigma}(\omega) = -\frac{1}{\pi}\text{Im}G_{\mathbf{k},\sigma}(\omega)$, $\eta \rightarrow 0$, is the momentum resolved spectral function. In ultracold gas experiments, $\rho_{\mathbf{k},\sigma}(\omega)$ can be measured directly by momentum resolved photo-emission spectroscopy [35–37]. For an impurity concentration $n_{\text{imp}}/N_a \approx 0.03$ and parameters corresponding to $\varepsilon_b/\pi\Gamma = -0.21$ in Fig. 2 (a), we show $\rho_{\mathbf{k},\sigma}(\omega)$ in Fig. 2 (b). The change of the height and width of the peaks when approaching k_F can be easily understood as due to the coupling of the itinerant states to the Kondo resonance. In Eq. (14) the imaginary part of $G_{b,\sigma}(\omega)$, which is proportional to the spectral function $\rho_{b,\sigma}(\omega)$ leads to a broadening of the spectral function, which is most pronounced close to $\varepsilon_{\mathbf{k}} = \varepsilon_F$, where the Kondo resonance lies. This is a striking feature opposite to usual scattering mechanisms which increase when moving away from the Fermi energy. In fact, we can interpret this as a self-energy term, $\Sigma(\omega) = n_{\text{imp}}V_\sigma^2 G_{b,\sigma}(\omega)$, and this can be extracted [57] by well established tech-

niques developed in angle-resolved photo emission spectroscopy [38, 39]. Hence, this procedure gives access to the spectral function in Fig. 2 (a) and as such is a direct signature of the Kondo peak. More conventional radio frequency (rf) spectroscopy can also provide explicit signatures of the Kondo-correlated state. As discussed comprehensively in the SM the signal shows characteristic broadened peaks, which are shifted from the ones for a system without the Kondo effect. Also spectroscopy of the species b impurity atom, switching from an uncorrelated state to a Kondo state, would be very interesting. Characteristic power law tails can be observed as discussed in detail in Refs. [40, 41].

Addressing open questions - We discuss now a number of interesting questions, which can be addressed once the Kondo-correlated state has been realized. It has been long argued [11] that the magnetically screened impurity should be surrounded by a screening cloud with the spatial extension of order $\xi_K = \frac{\hbar v_F}{k_B T_K}$. However, experimentally it has not been possible to provide firm evidence for the Kondo cloud, such that its existence is unclear. A typical quantity to show Kondo cloud features is the decay of the equal time spin correlation function $\langle S_c(\mathbf{r})s_{\text{imp}} \rangle$, which is difficult to access in condensed matter systems. In contrast, in the proposed ultracold gas system this correlation function should become accessible by spectroscopic tools [42], such that ξ_K could be determined and this fundamental question of Kondo physics be settled. Since our setup allows to switch the impurity on and off by optically changing the hyperfine state of the b species, it would also be curious to analyze the time scale on which the Kondo cloud builds up. The proposed setup has also great potential to shed light on a number of intriguing issues for the Kondo lattice including the observation of a fractionalized Fermi liquid (FL*) phase [43] and the occurrence of superconductivity close to a quantum phase transitions.

Conclusions - We have demonstrated how to realize a Kondo-correlated state for a mixture of ultracold atoms. The proposed setup, different from a previous proposal based on alkaline-earth atoms [44], ones related to the spin-Boson model [45, 46] and a bosonic form [47], can be realized with experimental techniques currently available. In general, this allows one to analyze field dependent and anisotropic Kondo physics. We proposed the recently studied Na-K-mixture as a suitable system and computed the rf response in a regime well accessible by experiments. There are numerous possible extension of our work including the study of non-equilibrium Kondo physics, Kondo lattice systems and signatures of quantum criticality. We point out that geometrical resonances which we discuss in the supplementary material can also appear in $l > 0$ angular momentum channels even for purely s-wave scattering between localized and itinerant atoms (see e.g. [24, 25]). This may open interesting possibilities for realizing multichannel Kondo physics.

Acknowledgments - We wish to thank S. Blatt, S. Gopalakrishnan, A.C. Hewson, M. Koehl, Y. Oreg, M. Punk, S. Will, A. Tselik, G. Zarand, F. Zhou, and M. Zwierlein for helpful discussions. We would like to thank Martin Zwierlein for pointing out to us the possibility of using Feshbach bound states on impurity atoms to realize the Kondo effect in cold atomic systems and for a collaboration on related projects [48]. JB acknowledges financial support from the DFG through grant number BA 4371/1-1. We also acknowledge support from Harvard-MIT CUA, DARPA OLE program, AFOSR Quantum Simulation MURI, AFOSR MURI on Ultracold Molecules, the ARO-MURI on Atomtronics, ARO MURI Quism program and the EU ERC Ferlodim.

S1 Hybridization function

The hybridization function was defined as,

$$K_\sigma(\omega) = \sum_{\mathbf{k}} \frac{|V_{\mathbf{k},\sigma}|^2}{\omega + i\eta - \varepsilon_{\mathbf{k}} + \mu}. \quad (15)$$

We write $K_\sigma(\omega) = \Lambda_\sigma(\omega) - i\Gamma_\sigma(\omega)$. If we assume that $V_{\mathbf{k},\sigma} = V_\sigma$ is constant and is cut off by $\Lambda_{v,\sigma}$, then the imaginary part becomes,

$$\Gamma_\sigma(\omega) = -\pi |V_{\omega,\sigma}|^2 \rho_0(\omega + \mu) \theta(\omega + \mu) \theta(\Lambda_{v,\sigma} - \mu - \omega). \quad (16)$$

The real part can also be evaluated in terms of principle value integrals and we find for $\omega < -\mu$,

$$\Lambda_\sigma^<(\omega) = -2|V_\sigma|^2 c_3 \left[\sqrt{\Lambda_{v,\sigma}} - \sqrt{-\omega - \mu} \arctan\left(\frac{\Lambda_{v,\sigma}}{-\omega - \mu}\right) \right]. \quad (17)$$

and for $\omega > -\mu$,

$$\Lambda_\sigma^>(\omega) = -2|V_\sigma|^2 c_3 \left[\sqrt{\Lambda_{v,\sigma}} - \frac{1}{2} \sqrt{\omega + \mu} \log\left(\frac{\sqrt{\Lambda_{v,\sigma}} + \sqrt{\omega + \mu}}{\sqrt{\Lambda_{v,\sigma}} - \sqrt{\omega + \mu}}\right) \right].$$

The function is continuous at $\omega \rightarrow -\mu$ but not smooth. A schematic plot with $\mu = \varepsilon_F$ is shown in Fig. 3.

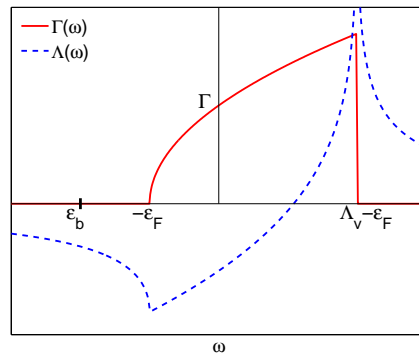


FIG. 3: (Color online) Schematic plot of the hybridization function $\Gamma(\omega)$ and $\Lambda(\omega)$ indicating the boundaries of the continuum states $-\varepsilon_F$ and upper cutoff Λ_v and the energy of the bare bound state ε_b , generally below the continuum. At the sharp positive edge $\Lambda(\omega)$ has a logarithmic singularity. This can lead to bound states outside the continuum [49]. The sharp cut-off can be softened without changing any of the results qualitatively. For simplicity we have omitted the index σ .

S2 Kondo physics with additional resonances

In the main text it was discussed how the system of ^{40}K and ^{23}Na atom can be tuned into a Kondo-correlated state employing two Feshbach resonances. It is fortunate

in this situation that the effective scattering lengths intersect in a suitable regime as show in Fig. 1(b). However, for other systems this will not generally be the case. For instance, two hyperfine states of ${}^6\text{Li}$ have a number of Feshbach resonances with ${}^{133}\text{Cs}$ between 800-900G with promising features [21], but the intersection does not directly lie in a suitable regime. Here we show that it can nevertheless be possible to tune the system into a Kondo-correlated state with the help of confinement induced additional resonances [23, 24].

To see how the confining potential can help to align the bound state energies in the right regime, we consider for each component σ the two-particle scattering problem between species a and b . Without the harmonic confinement ($\omega_{\text{ho}} = 0$) the scattering problem for each σ is characterized by the bare s-wave scattering length $a_{0,\sigma}$. For $a_{0,\sigma} > 0$, the effective scattering length a_σ is found to have many sharp resonances [24], which can be understood as follows. A molecular bound state, where only b feels the confinement has the harmonic oscillator energy $E_n = (2n + \frac{3}{2})\sqrt{\frac{m_b}{M}}\hbar\omega_{\text{ho}}$, with $M = m_a + m_b$. This energy reduced by the binding energy $E_{b,\sigma}$ can become resonant with the ground state energy of oscillator and atom, $E_n + E_{b,\sigma} = 3/2\hbar\omega_{\text{ho}}$, which leads to the resonance for the effective scattering length a_σ . From this we obtain the condition [24],

$$a_{0,\sigma}^{\text{res}}(n) = \frac{a_{\text{ho}}}{\sqrt{\frac{2m_r}{m_b}}\sqrt{(2n + \frac{3}{2})\sqrt{\frac{m_b}{M}} - \frac{3}{2}}} \quad (18)$$

where $n = 1, 2, \dots$. Hence, in a situation where one scattering length is in suitable regime the second one can be tuned there by one of those additional resonances.

In Fig. 4 (a) we show schematically the bare scattering lengths $a_{0,\sigma}$ close to Feshbach resonances. We have also indicated values of the magnetic field where the resonance condition, Eq. (18), is satisfied.

Now let us assume that on tuning B we have satisfied $c_l < k_F a_\downarrow(B_K) < c_u$, but $k_F a_\uparrow(B_K) < c_l$ [see Fig. 4 (b)]. Then one can change ω_{ho} by the laser power to bring a sharp resonance in the vicinity, i.e., change a_{ho} such that $a_0(B_K) \simeq a_0^{\text{res}}(n_K)$ for some n_K . Then some further fine tuning to $B_K - \delta B$ will satisfy the condition $a_\downarrow(B_K - \delta B) = a_\uparrow(B_K - \delta B)$, such that conditions (I) and (II) are satisfied [see Fig. 4 (c)]. Since we have used the additional resonance we have $r_{e,\uparrow} \neq r_{e,\downarrow}$, and thus in general $h, \Delta\Gamma \neq 0$. There are two different cases to be considered: (i) $|r_{e,\sigma}| \ll a_\sigma$, in this case, $\Delta\Gamma \approx 0$ and $h \approx 0$, such that conditions (I-III) are satisfied. Note that $r_{e,\sigma}$ can be reduced by decreasing a_{ho} as seen in Eq. (3). (ii) $|r_{e,\sigma}| \sim a_\sigma$ or $|r_{e,\sigma}| > a_\sigma$, in this case we have to tune B further to satisfy the condition (III), $\Delta\Gamma = \alpha_h h$. We can focus on the fast variation of a_\uparrow close to the resonance, and assume the other quantities in this regime as constant. Depending on the strength of the asymmetry $r_{e,\uparrow}/r_{e,\downarrow}$ a solution which still respects Eq. (12) can be

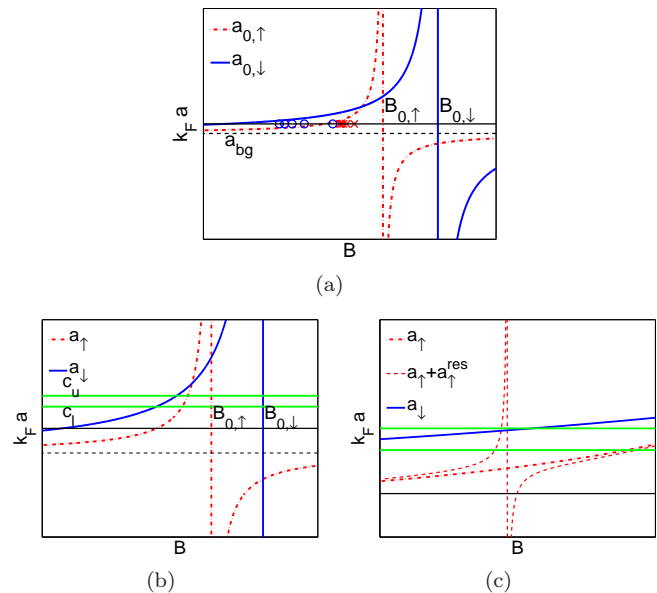


FIG. 4: (Color online) (a) Schematic plot of the bare scattering length $a_{0,\sigma}$ for two interspecies Feshbach resonances, with $B_{0,\uparrow} < B_{0,\downarrow}$, and $|\Delta B_{0,\uparrow}| < |\Delta B_{0,\downarrow}|$, $\Delta B_{0,\sigma} < 0$, $a_{\text{bg}} < 0$. The circles (crosses) indicate the first 5 magnetic fields where the resonance condition in Eq. (18) is satisfied for $a_{0,\downarrow}$ ($a_{0,\uparrow}$). (b) Schematic plot of the effective scattering length a_σ for a situation where the condition $a_\uparrow = a_\downarrow$ is not satisfied within the Kondo boundaries (c_l, c_u). (c) Close-up of (b), where a resonance has been tuned to $B = B_K$.

found.

S3 Properties of the AIM and mapping to the Kondo model

Here we discuss some properties of the AIM in Eq. (5). First, we show how an effective magnetic field emerges for the case $V_\uparrow \neq V_\downarrow$. This is seen directly from the scaling equations for the Anderson model [11, 50]. For a general DOS one finds,

$$\frac{dh}{d\Lambda} = \frac{1}{2\pi} \left[\frac{\Gamma_\uparrow(\Lambda)}{\Lambda - \varepsilon_{b,\uparrow}} - \frac{\Gamma_\downarrow(\Lambda)}{\Lambda - \varepsilon_{b,\downarrow}} + \frac{\Gamma_\downarrow(-\Lambda)}{\Lambda + \varepsilon_{b,\downarrow} + U} - \frac{\Gamma_\uparrow(-\Lambda)}{\Lambda + \varepsilon_{b,\uparrow} + U} \right].$$

We introduced $\Gamma_\sigma(\Lambda) = \Gamma_\sigma \rho_0(\Lambda + \mu)$. When considering the situation $U \rightarrow \infty$ the last two terms can be neglected. In the special case of a particle-hole symmetric model, $\varepsilon_b = -U/2$, $\varepsilon_b = (\varepsilon_{b,\uparrow} + \varepsilon_{b,\downarrow})/2$, with symmetric and constant DOS, $\rho_0 = 1/W$, and initially zero field $h = 0$, no effective field is generated. We can see this from

$$\frac{dh}{d\Lambda} = \frac{\Gamma_\uparrow - \Gamma_\downarrow}{2\pi} \frac{2\varepsilon_b + U}{(\Lambda + \varepsilon_b + U)(\Lambda - \varepsilon_b)}, \quad (19)$$

where the right hand side vanishes in the particle hole symmetric case. In all other cases for $\Gamma_\uparrow \neq \Gamma_\downarrow$ an effective field h_{eff} is generated as a second order effect in the

hybridization. From Eq. (19) we can see that the effective field is proportional to $\Delta\Gamma$, such that the form $\Delta\Gamma = \alpha_h h$ to offset the field is appropriate. We see that for $\Delta\Gamma > 0$, $U + 2\varepsilon_b > 0$ reducing Λ leads to a negative h_{eff} . Hence, $\alpha_h > 0$ in the offset equation, which is opposite to the convention in Ref. [31]. The above argument is valid if the hybridization cut-offs $\Lambda_{v,\sigma}$ are equal. However, for $\Lambda_{v,\uparrow} > \Lambda_{v,\downarrow}$, we find that in the regime $\Lambda \in (\Lambda_{v,\downarrow}, \Lambda_{v,\uparrow})$, $h(\Lambda)$ decreases, since $\Gamma_{\downarrow}(\Lambda) = 0$. This has to be taken into account, when the effective field h_{eff} is computed.

To understand the specific Kondo properties it is convenient to map the AIM in Eq. (5) to a Kondo model by a Schrieffer-Wolff transformation [51]. The transformed Hamiltonian is

$$H' = H_0 + \frac{1}{2}[S, H_1] + \dots \quad (20)$$

H_1 is the hybridization term and higher order terms contain higher powers in $V_{\mathbf{k},\sigma}$. The explicit choice of the generator is,

$$S = \sum_{\mathbf{k},\sigma} \left[\left(\frac{V_{\mathbf{k},\sigma}}{\varepsilon_{\mathbf{k}} - \varepsilon_{b,\sigma}} (1 - n_{b,-\sigma}) c_{\mathbf{k},\sigma}^\dagger c_{b,\sigma} - \text{h.c.} \right) + \left(\frac{V_{\mathbf{k},\sigma}}{\varepsilon_{\mathbf{k}} - \varepsilon_{b,\sigma} - U} n_{b,-\sigma} c_{\mathbf{k},\sigma}^\dagger c_{b,\sigma} - \text{h.c.} \right) \right].$$

This includes projection operators for the occupation of the site. Evaluating the commutator yields the interaction term of the transformed Hamiltonian,

$$H_{\text{int}} = \sum_{\mathbf{k},\mathbf{k}'} [J_{\mathbf{k},\mathbf{k}',\uparrow,\downarrow} S^+ c_{\mathbf{k},\downarrow}^\dagger c_{\mathbf{k}',\uparrow} + J_{\mathbf{k},\mathbf{k}',\uparrow,\downarrow} S^- c_{\mathbf{k},\uparrow}^\dagger c_{\mathbf{k}',\downarrow} + S_z J_{\mathbf{k},\mathbf{k}',z} (c_{\mathbf{k},\uparrow}^\dagger c_{\mathbf{k}',\uparrow} - c_{\mathbf{k},\downarrow}^\dagger c_{\mathbf{k}',\downarrow})].$$

Here, \mathbf{S} is the effective impurity spin, $S_i = \frac{1}{2} c_{b,\sigma}^\dagger \sigma_{\sigma\sigma'}^{(i)} c_{b,\sigma'}$, $S^\pm = S_1 \pm iS_2$. We have introduced,

$$J_{\mathbf{k},\mathbf{k}',\sigma,\sigma'} = \frac{V_{\mathbf{k},\sigma} V_{\mathbf{k}',\sigma'}^*}{2} \left(\frac{1}{\varepsilon_{\mathbf{k}} - \varepsilon_{b,\sigma}} + \frac{1}{\varepsilon_{\mathbf{k}'} - \varepsilon_{b,\sigma'}} - \frac{1}{\varepsilon_{\mathbf{k}} - \varepsilon_{b,\sigma} - U} - \frac{1}{\varepsilon_{\mathbf{k}'} - \varepsilon_{b,\sigma'} - U} \right).$$

Often one uses $\varepsilon_{\mathbf{k}}, \varepsilon_{\mathbf{k}'} \simeq 0$ such that the expressions simplify. Note that $J_{\mathbf{k},\mathbf{k}',\uparrow,\downarrow} = J_{\mathbf{k}',\mathbf{k},\downarrow,\uparrow}$, so that H_{int} is hermitian. The first two terms are spin-flip terms of a spin with the conduction band electrons. We also have an additional term which behaves like an effective magnetic field,

$$H_{\text{mag}} = S_z \sum_{\mathbf{k},\mathbf{k}'} [\Delta J_{\mathbf{k},\mathbf{k}',z} (c_{\mathbf{k},\uparrow}^\dagger c_{\mathbf{k}',\uparrow} + c_{\mathbf{k},\downarrow}^\dagger c_{\mathbf{k}',\downarrow}) - (W_{\mathbf{k},\mathbf{k}',\uparrow} - W_{\mathbf{k},\mathbf{k}',\downarrow})]. \quad (22)$$

where $\Delta J_{\mathbf{k},\mathbf{k}',z} = \frac{1}{2} (J_{\mathbf{k},\mathbf{k}',\uparrow,\uparrow} - J_{\mathbf{k},\mathbf{k}',\downarrow,\downarrow})$ and $W_{\mathbf{k},\mathbf{k}',\sigma}$ is given by,

$$W_{\mathbf{k},\mathbf{k}',\sigma} = \frac{V_{\mathbf{k},\sigma} V_{\mathbf{k}',\sigma}^*}{2} \left(\frac{1}{\varepsilon_{\mathbf{k}} - \varepsilon_{b,\sigma}} + \frac{1}{\varepsilon_{\mathbf{k}'} - \varepsilon_{b,\sigma}} \right). \quad (23)$$

This term vanishes for a symmetric model $\varepsilon_b = -U/2$, a symmetric DOS and $V_{\uparrow} = V_{\downarrow}$. However, in general it is finite and acts like a local magnetic field as discussed above for the AIM. Generally, there are also terms $\sim c_{b,\sigma}^\dagger c_{b,-\sigma}^\dagger$, which change the impurity occupation by 2. In the regime of single occupancy they are neglected. We also take the Kondo couplings independent of \mathbf{k} . We define $J_{\perp} = J_{\uparrow,\downarrow} = J_{\downarrow,\uparrow}$ and $J_z = (J_{\uparrow,\uparrow} + J_{\downarrow,\downarrow})/2$,

$$J_{\perp} = \frac{V_{\uparrow} V_{\downarrow}}{2} \left(\frac{1}{-\varepsilon_{b,\uparrow}} + \frac{1}{-\varepsilon_{b,\downarrow}} \right), \quad J_z = \frac{1}{2} \left(\frac{V_{\uparrow}^2}{-\varepsilon_{b,\uparrow}} + \frac{V_{\downarrow}^2}{-\varepsilon_{b,\downarrow}} \right).$$

In general $J_{\perp} \neq J_z$ and hence we have to deal with an anisotropic Kondo model.

S4 Scaling of the anisotropic Kondo model and T_K

We can define the Kondo scale T_K where J_z diverges in the scaling equations [11, 52]. In the isotropic case for constant DOS, the result is

$$T_{0,K} = \Lambda_0 e^{-\frac{1}{2\rho_0 J}}. \quad (24)$$

Here, Λ_0 is a suitable high energy cutoff. The square root DOS of the three dimensional systems leads to minor modifications which can be included in a prefactor. In the anisotropic case the equations read,

$$\frac{dJ_z}{d \log(\Lambda)} = -[\rho_0(\Lambda + \mu) + \rho_0(-\Lambda + \mu)] J_{\perp}^2, \quad (25)$$

$$\frac{dJ_{\perp}}{d \log(\Lambda)} = -[\rho_0(\Lambda + \mu) + \rho_0(-\Lambda + \mu)] J_{\perp} J_z. \quad (26)$$

Using $J_z^2 - J_{\perp}^2 = C$, the Kondo scale T_K is found to be

$$T_K = \alpha_K \Lambda_0 e^{-\frac{\gamma}{2\rho_0 J_0}}, \quad \gamma = \frac{\text{atanh}(\sqrt{1-x^2})}{\sqrt{1-x^2}}, \quad (27)$$

for $x = J_{\perp}/J_z < 1$ and $\gamma = \frac{\text{atan}(\sqrt{x^2-1})}{\sqrt{x^2-1}}$ for $x > 1$. The coefficient α_K accounts for the varying DOS and possibly different upper and lower cutoffs.

Having established these relations, we can derive a condition for J_z , such that T_K is of the order of the experimental temperature (see main text). It can be written in the form $-1/2 \sum_{\sigma} \varepsilon_{b,\sigma} / (\pi \Gamma_{\sigma}) < c_2$. If one assume that the asymmetry is not very large, that is $x > 1/2$ in Eq. (27), one can find the estimate $c_2 \approx 0.6$.

S4 NRG calculations for bound state spectral functions

We have done NRG calculations for the AIM in Eq. (5) and computed the low temperature bound state spectral function $\rho_{b,\sigma}(\omega)$. The ω -dependence of $K_{\sigma}(\omega)$ is dealt with as in NRG applications for dynamical mean field

calculations [34]. The first set of parameter is for the situation, where $B = B_s$ in Eq. (13) and we vary k_F/k_F^0 , where $k_F^0 = 1.6 \cdot 10^{-4}/a_B$. The parameters are calculated as follows: a_σ and $r_{e,\sigma}$ are calculated from Eq. (3), and the AIM model parameters $\varepsilon_{b,\sigma}/\varepsilon_F$, and V_σ/ε_F are computed from Eq. (10) and Eq. (9). The ratio $\frac{-\varepsilon_{b,\sigma}}{\pi\Gamma_\sigma}$ is given in Eq. (11), the upper cutoff $\Lambda_{v,\sigma} = \frac{\varepsilon_F}{(k_F a_\sigma)^2}$, and $\varepsilon_F = 1$ sets the energy scale in the calculations. We chose U large enough that double occupancy is strongly suppressed. The numerical values for the parameters are given in Table I. The value for V_σ corresponds to the choice $V_0 k_F^3 = 1000$.

k_F/k_F^0	$k_F a_\sigma$	$\varepsilon_{b,\sigma}/\varepsilon_F$	V_σ/ε_F	$-\varepsilon_{b,\sigma}/(\pi\Gamma_\sigma)$
1	0.55	-1.64	0.177	0.21
0.75	0.41	-2.92	0.204	0.28
0.45	0.25	-8.11	0.264	0.47

TABLE I: Values for the AIM model parameters, when varying the density.

$B(G)$	$k_F a_\uparrow$	$k_F a_\downarrow$	$\varepsilon_b/\varepsilon_F$	h/ε_F	V_\uparrow/ε_F	$V_\downarrow/\varepsilon_F$	$\Delta\Gamma/\varepsilon_F$
106.25	0.55	0.55	-1.64	0.000	0.177	0.177	0.000
106.2	0.48	0.53	-1.78	-0.075	0.174	0.176	-0.029
106.1	0.38	0.50	-1.96	-0.175	0.167	0.175	-0.111
106.0	0.30	0.47	-2.12	-0.243	0.157	0.174	-0.219

TABLE II: Values for the AIM model parameters, when varying the magnetic field B .

$k_F a_\uparrow$	$k_F a_\downarrow$	$\varepsilon_b/\varepsilon_F$	h/ε_F	V_\uparrow/ε_F	$V_\downarrow/\varepsilon_F$	$\Delta\Gamma/\varepsilon_F$
0.53	0.53	-1.65	0.053	0.171	0.176	-0.077
0.51	0.53	-1.69	0.011	0.172	0.176	-0.060
0.49	0.53	-1.74	-0.037	0.173	0.176	-0.042

TABLE III: Values for the AIM model parameters close to the resonance for a_\uparrow .

The results for these calculation with varying k_F are shown in Fig. 2(a) in the main text. As discussed the bound state peaks lie between $-8\varepsilon_F$ and $-2\varepsilon_F$. Since renormalization effects can shift the energy from $\varepsilon_{b,\sigma} \rightarrow \bar{\varepsilon}_{b,\sigma}$, the solution of $\text{Re}G_{b,\sigma}(\omega)^{-1} = 0$, the bound state level can be shifted from their bare values $\varepsilon_{b,\sigma}$ to lower energies. Due to interaction effects the peaks are broadened, even though they lie outside the continuum. We see a clear many-body Kondo peak at $\omega = 0$. When increasing $-\varepsilon_{b,\sigma}/(\pi\Gamma)$ the width of the resonance does not decrease very much. The reason for this is that there are two competing effects. The first is that the bare width $\pi\Gamma$ is increasing for the set of parameters (7.8, 10.4, 17.4). However, the state for $k_F a_\sigma = 0.25$ has a substantially smaller renormalization factor ($z = 0.02$) than the one for $k_F a_\sigma = 0.55$ ($z = 0.13$). Taking into account both of these effects one understands that the width of the Kondo peak, which is proportional to $z\Gamma$, does not change very much.

In Table II the parameters are shown for the situation where the field is reduced from $B_s = 106.25\text{G}$ and $k_F = k_F^0$ is held fixed. The corresponding spectral functions are shown in Fig. 5.

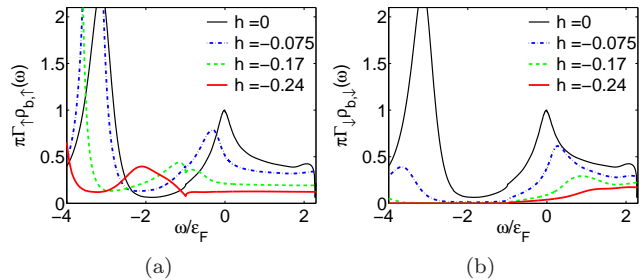


FIG. 5: (Color online) Spin resolved spectral functions $\rho_{b,\uparrow}(\omega)$ (a) and $\rho_{b,\downarrow}(\omega)$ (b) for decreasing magnetic field $B = 106.25, 106.2, 106.1, 106\text{G}$, which yields a number of different values for the $k_F a_\sigma$ and the field h and the other model parameters (see Table II), where $\Delta\Gamma \neq 0$. The Kondo resonance is split and suppressed.

The spectral functions show typical behavior of the AIM in a magnetic field [53–55]. We see that $\rho_{b,\uparrow}(\omega)$ gains spectral weight at $\omega < 0$ on decreasing the field h , and the Kondo peak is shifted to negative energies. In contrast, there is a reduction of spectral weight for $\omega < 0$ in $\rho_{b,\downarrow}(\omega)$ when h becomes larger. At the same time the Kondo peak is shifted to positive energies and broadened. Note that $\Delta\Gamma < 0$ can reduce the magnetic field effect.

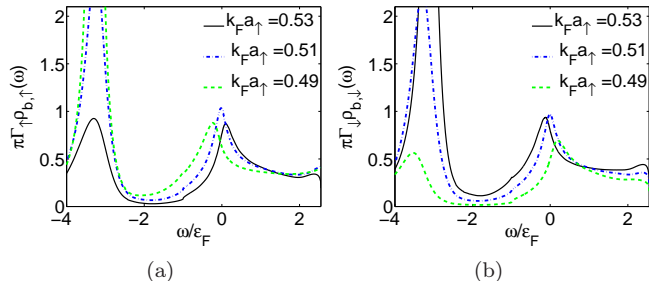


FIG. 6: (Color online) Spectral functions $\rho_{b,\uparrow}(\omega)$ and (b) $\rho_{b,\downarrow}(\omega)$ close to a resonance for a number of different values of $k_F a_\uparrow$ and the complete set of AIM parameters is given in Table III.

For illustration we also discuss a case where the additional resonances are used to tune into the Kondo-correlated state (cf. Fig. 4). We analyze the K-Na system and use $B = 106.2\text{G} < B_s$, where from Eq. (3) $k_F a_\downarrow = 0.475$ and $k_F a_\uparrow = 0.53$. Then we tune $k_F a_\uparrow$ with the additional resonance as discussed in Fig. 4(b,c) to satisfy conditions (I-III). The model parameters are given in Table III. We have for $B_K = 106.2\text{G}$ and $a_{\text{ho}} = 3.12 \cdot 10^3 a_B$, the closest resonance at $n_K \approx 6$. We could also employ the resonance at a different value n_K by suitably adjusting ω_{ho} and hence a_{ho} . We have assumed that $k_F a_\downarrow = 0.53$, $k_F r_{e,\uparrow} = 0.52$, $k_F r_{e,\downarrow} = 0.47$ are

held constant and only $k_F a_\uparrow$ varies close to the resonance. Similar tuning is possible for other values of B and a_{ho} . Generically, for $a_{0,\uparrow} < a_{0,\downarrow}$ one has $|r_{e,\uparrow}| > |r_{e,\downarrow}|$, which leads to $\Delta\Gamma < 0$ and $h > 0$. This leads to the expectation value $n_\uparrow - n_\downarrow < 0$. Now decreasing a_\uparrow close to the resonance from $a_\uparrow \simeq a_\downarrow$ leads to decreasing h , increasing $\Delta\Gamma$, and $\Lambda_{v,\uparrow} > \Lambda_{v,\downarrow}$. This will lead eventually to a situation, where the field effect is canceled such that $n_\uparrow - n_\downarrow \simeq 0$. Since in this situation still $V_\uparrow \neq V_\downarrow$, in general anisotropic Kondo physics is realized.

The results for the spectral functions are shown in Fig. 6. We identify a clear Kondo peak close to $\omega = 0$. The other features are typical for the Kondo effect in a magnetic field with a slightly shifted resonance and shifted spectral weight. For $k_F a_\uparrow \simeq 0.51 < k_F a_\downarrow$ the field effect is roughly canceled and $\rho_{b,\uparrow}(\omega) \sim \rho_{b,\downarrow}(\omega)$.

S5 RF spectroscopy and experimental signature

A well-established experimental technique for ultracold atomic gases is radio frequency (rf) spectroscopy. The transition rate from a hyperfine state $|\sigma, \mathbf{k}\rangle$ to a different one $|\mathfrak{3}, \mathbf{k}\rangle$, which does not interact with others and is initially unoccupied, is given by [48],

$$I_\sigma(\omega) = \frac{\Omega^2}{(2\pi)^4} \int d^3k \int d\omega' \rho_{\mathbf{k},\sigma}(\omega') \rho_{\mathfrak{3},\mathbf{k}}(\omega + \omega') n_F(\omega'). \quad (28)$$

Ω is the intensity and ω the rf frequency. We assume that $|\mathfrak{3}, \mathbf{k}\rangle$ is a free state shifted in energy by $\omega_{3,\sigma}$ with respect to the $|\sigma, \mathbf{k}\rangle$ states, $\rho_{\mathfrak{3},\mathbf{k}}(\omega) = \delta(\omega - (\xi_{\mathbf{k}} + \omega_{3,\sigma}))$. The spectral function for $G_{b,\sigma}(\omega)$ in Eq. (14) reads

$$\rho_{\mathbf{k}}(\omega) = \frac{(\eta + n_{\text{imp}} V_\sigma^2 \pi \rho_{b,\sigma}(\omega)) / \pi}{\left(\omega - \xi_{\mathbf{k}} - n_{\text{imp}} V_\sigma^2 G_{b,\sigma}^R(\omega) \right)^2 + \left(\eta + n_{\text{imp}} V_\sigma^2 \pi \rho_{b,\sigma}(\omega) \right)^2}. \quad (29)$$

We see that the real part $G_{b,\sigma}^R(\omega)$ can contribute to a shift of the dispersion and the imaginary part gives an additional broadening. All terms in Eq. (28) depend on \mathbf{k} via $\varepsilon_{\mathbf{k}}$ so we can introduce a density of states (DOS) $\rho_0(\varepsilon)$ and write,

$$I_\sigma(\omega) = \frac{\Omega^2}{2\pi} \int d\varepsilon \rho_0(\varepsilon) \rho_{\varepsilon,\sigma}(\varepsilon - \mu + \omega_{3,\sigma} - \omega) n_F(\varepsilon - \mu + \omega_{3,\sigma} - \omega). \quad (30)$$

In the limit of low temperature this becomes,

$$I_\sigma(\omega) = \frac{\Omega^2}{2\pi} \int_{-\infty}^{\omega - \omega_{3,\sigma}} d\varepsilon \rho_0(\varepsilon + \mu) \rho_{\varepsilon + \mu, \sigma}(\varepsilon + \omega_{3,\sigma} - \omega). \quad (31)$$

In the case of non-interaction fermions, $\rho_{\varepsilon + \mu, \sigma}(\varepsilon + \omega_{3,\sigma} - \omega) = \delta(\varepsilon + \omega_{3,\sigma} - \omega - \varepsilon) = \delta(\omega_{3,\sigma} - \omega)$, so the RF spectrum

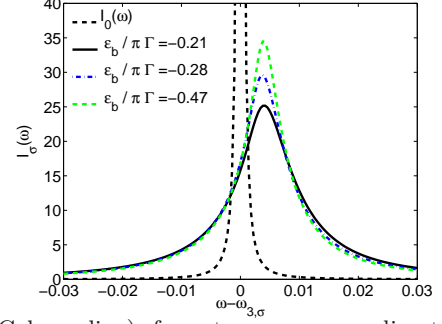


FIG. 7: (Color online) rf spectrum corresponding to the spectral function in Fig. 2(a) in the main text and the values in Table I. We also show $I_0(\omega)$, (broadened delta-function) for comparison.

reads,

$$I_0(\omega) = \frac{2}{3} \frac{\Omega^2}{2\pi} k_F^3 \delta(\omega_{3,\sigma} - \omega). \quad (32)$$

The rf spectra can be understood as the sum of all the transitions from the modified band dispersion $E_{\mathbf{k},\sigma}$ with a certain width $\Delta_{\mathbf{k},\sigma}$ for $|\sigma, \mathbf{k}\rangle$, to a non-interacting dispersion $\varepsilon_{\mathbf{k}}$ shifted by $\omega_{3,\sigma}$ ($|\mathfrak{3}, \sigma\rangle$). A shift in the dispersion gives a shift of the rf signal, flattening of the dispersion can give additional weight at higher or lower energies, and broadening leads to a broadened rf signal. The Kondo peak on its own leads to a band bending and broadening and hence a rf peak which is shifted and has high energy tails.

The rf signal corresponding to Fig. 2(a) in the main text for an impurity concentration $n_{\text{imp}}/N_a \approx 0.03$ is shown in Fig. 7.

When comparing $I_\sigma(\omega)$ to the unperturbed signal $I_0(\omega)$ we find a broadened peak slightly shifted from $\omega = \omega_{3,\sigma}$. This shape can be traced back to the effect of the coupling of the itinerant states to the bound state spectral function. In Eq. (29) this leads to a broadening of the spectral function and a small band bending close to $\varepsilon_{\mathbf{k}} = \varepsilon_F$, where the Kondo resonance lies. The signal in $I_\sigma(\omega)$ narrows for decreasing Kondo scale due to the reduced modification of $\rho_{\mathbf{k},\sigma}(\omega)$. The signals in Fig. 7 are rather characteristic for the two peak structure in Fig. 2(a), such that the Kondo-correlated state and position of the Kondo resonance can be identified well with rf spectroscopy.

In Fig. 8 we show the rf spectra when varying B corresponding to the results in Fig. 5.

The peak in $I_\uparrow(\omega)$ is shifted to lower energies. This can be understood looking at the effect of the moving of the Kondo peak to lower energies and its effect on $\rho_{\mathbf{k},\uparrow}(\omega)$. In contrast, we find that $I_\downarrow(\omega)$ reverts to the non-interacting result $I_0(\omega)$ as the B field makes the relevant features disappear in the spectral function $\rho_{b,\downarrow}(\omega)$ and thus $\rho_{\mathbf{k},\downarrow}(\omega)$. The careful analysis of the $I_\sigma(\omega)$ signals as function of magnetic field should provide a good picture of the tuning into the Kondo-correlated state.

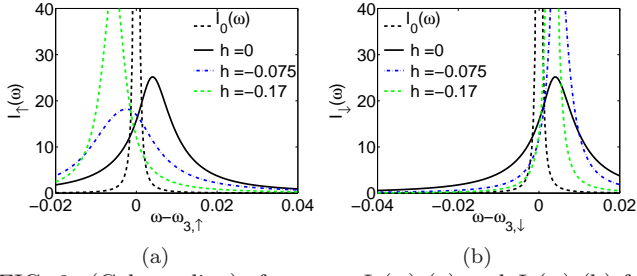


FIG. 8: (Color online) rf spectra $I_{\uparrow}(\omega)$ (a) and $I_{\downarrow}(\omega)$ (b) for decreasing magnetic field B as in Fig. 5 and model parameters in Table II. We also show $I_0(\omega)$, (broadened delta-function) for comparison.

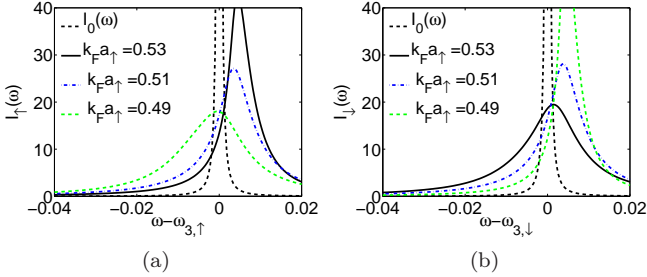


FIG. 9: (Color online) rf spectra $I_{\uparrow}(\omega)$ (a) and $I_{\downarrow}(\omega)$ (b) close to a resonance for a number of different values of $k_F a_{\uparrow}$ as in Fig. 6 and the complete set of AIM parameters is given in Table III. We also show $I_0(\omega)$, (broadened delta-function) for comparison.

The rf signal corresponding to Fig. 6(a)(b) is shown in Fig. 9(a)(b). When comparing $I_{\sigma}(\omega)$ to $I_0(\omega)$ we find a broadened peak slightly shifted from $\omega = \omega_{3,\sigma}$. Again we can understand the shape from the form of the spectral function and its effect on the itinerant states in Eq. (29). The signal in $I_{\uparrow}(\omega)$ broadens and shifts to smaller ω on decreasing $k_F a_{\uparrow}$, and the opposite happens for $I_{\downarrow}(\omega)$.

-
- [1] I. Bloch, J. Dalibard, and W. Zwerger, *Rev. Mod. Phys.* **80**, 885 (2008).
- [2] W. Hofstetter, J. I. Cirac, P. Zoller, E. Demler, and M. D. Lukin, *Phys. Rev. Lett.* **89**, 220407 (2002).
- [3] M. Greiner, O. Mandel, T. Esslinger, T. W. Hansch, and I. Bloch, *Nature* **415**, 39 (2002).
- [4] M. Greiner, C. Regal, and D. Jin, *Nature* **426**, 537 (2003).
- [5] M. Zwierlein, J. Abo-Shaeer, A. Shirotzek, C. H. Schunck, and W. Ketterle, *Nature* **435**, 1047 (2005).
- [6] J. K. Chin, D. E. Miller, Y. Liu, C. Stan, W. Setiawan, C. Sanner, K. Xu, and W. Ketterle, *Nature* **443**, 961 (2006).
- [7] U. Schneider, L. Hackermuller, S. Will, T. Best, I. Bloch, T. A. Costi, R. W. Helmes, D. Rasch, and A. Rosch, *Science* **322**, 1520 (2008).
- [8] R. Jordens, N. Strohmaier, K. Gunter, H. Moritz, and T. Esslinger, *Nature* **455**, 204 (2008).
- [9] D. Goldhaber-Gordon, H. Shtrikman, D. Mahalu, D. Abusch-Magder, U. Meirav, and M. A. Kastner, *Nature* **391**, 156 (1998).
- [10] S. M. Cronenwett, T. H. Oosterkamp, and L. P. Kouwenhoven, *Science* **281**, 540 (1998).
- [11] A. C. Hewson, *The Kondo Problem to Heavy Fermions* (Cambridge University Press, Cambridge, 1993).
- [12] I. Affleck and P. Simon, *Phys. Rev. Lett.* **86**, 2854 (2001).
- [13] L. Borda, *Phys. Rev. B* **75**, 041307 (2007).
- [14] I. Affleck, L. Borda, and H. Saleur, *Phys. Rev. B* **77**, 180404 (2008).
- [15] Q. Si and F. Steglich, *Science* **329**, 1161 (2010).
- [16] H. v. Löhneysen, A. Rosch, M. Vojta, and P. Wölfle, *Rev. Mod. Phys.* **79**, 1015 (2007).
- [17] T. Köhler, K. Góral, and P. S. Julienne, *Rev. Mod. Phys.* **78**, 1311 (2006).
- [18] C. Chin, R. Grimm, P. Julienne, and E. Tiesinga, *Rev. Mod. Phys.* **82**, 1225 (2010).
- [19] J. W. Park, C.-H. Wu, I. Santiago, T. G. Tiecke, S. Will, P. Ahmadi, and M. W. Zwierlein, *Phys. Rev. A* **85**, 051602 (2012).
- [20] C.-H. Wu, J. W. Park, P. Ahmadi, S. Will, and M. W. Zwierlein, *Phys. Rev. Lett.* **109**, 085301 (2012).
- [21] S.-K. Tung, C. Parker, J. Johansen, C. Chin, Y. Wang, and P. S. Julienne, *Phys. Rev. A* **87**, 010702 (2013).
- [22] M. Repp, R. Pires, J. Ulmanis, R. Heck, E. D. Kuhnle, M. Weidemüller, and E. Tiemann, *Phys. Rev. A* **87**, 010701 (2013).
- [23] M. Olshanii, *Phys. Rev. Lett.* **81**, 938 (1998).
- [24] P. Massignan and Y. Castin, *Phys. Rev. A* **74**, 013616 (2006).
- [25] Y. Nishida and S. Tan, *Phys. Rev. A* **82**, 062713 (2010).
- [26] P. W. Anderson, *Phys. Rev.* **124**, 41 (1961).
- [27] E. Braaten and H.-W. Hammer, *Physics Reports* **428**, 259 (2006).
- [28] T. Kraemer, M. Mark, P. Waldburger, J. Danzl, C. Chin, B. Engeser, A. Lange, K. Pilch, A. Jaakkola, H.-C. Nägerl, et al., *Nature* **440**, 315 (2006).
- [29] N. Syassen, D. Bauer, M. Lettner, T. Volz, D. Dietze, J. Garcia-Ripoll, J. Cirac, G. Rempe, and S. Dürr, *Science* **320**, 1329 (2008).
- [30] J. Martinek, Y. Utsumi, H. Imamura, J. Barnaś, S. Maekawa, J. König, and G. Schön, *Phys. Rev. Lett.* **91**, 127203 (2003).
- [31] J. Martinek, M. Sindel, L. Borda, J. Barnaś, J. König, G. Schön, and J. von Delft, *Phys. Rev. Lett.* **91**, 247202 (2003).
- [32] M.-S. Choi, D. Sánchez, and R. López, *Phys. Rev. Lett.* **92**, 056601 (2004).
- [33] K. Wilson, *Rev. Mod. Phys.* **47**, 773 (1975).
- [34] R. Bulla, T. Costi, and T. Pruschke, *Rev. Mod. Phys.* **80**, 395 (2008).
- [35] T.-L. Dao, A. Georges, J. Dalibard, C. Salomon, and I. Carusotto, *Phys. Rev. Lett.* **98**, 240402 (2007).
- [36] J. Stewart, J. Gaebler, and D. Jin, *Nature* **454**, 744 (2008).
- [37] M. Feld, B. Fröhlich, E. Vogt, M. Koschorreck, and M. Köhl, *Nature* **480**, 75 (2011).
- [38] T. Valla, A. V. Fedorov, P. D. Johnson, B. O. Wells, S. L. Hulbert, Q. Li, G. D. Gu, and N. Koshizuka, *Science* **285**, 2110 (1999).
- [39] A. Damascelli, Z. Hussain, and Z.-X. Shen, *Rev. Mod. Phys.* **75**, 473 (2003).
- [40] C. Latta, F. Haupt, M. Hanl, A. Weichselbaum, M. Claassen, W. Wuester, P. Fallahi, S. Faelt, L. Glaz-

- man, J. von Delft, et al., *Nature* **474**, 627 (2011).
- [41] M. Knap, A. Shashi, Y. Nishida, A. Imambekov, D. A. Abanin, and E. Demler, *Phys. Rev. X* **2**, 041020 (2012).
- [42] M. Knap, A. Kantian, T. Giamarchi, I. Bloch, M. D. Lukin, and E. Demler, *ArXiv e-prints* (2013), 1307.0006.
- [43] T. Senthil, S. Sachdev, and M. Vojta, *Phys. Rev. Lett.* **90**, 216403 (2003).
- [44] A. Gorshkov, M. Hermele, V. Gurarie, C. Xu, P. Julienne, J. Ye, P. Zoller, E. Demler, M. Lukin, and A. Rey, *Nature Physics* **6**, 289 (2010).
- [45] A. Recati, P. O. Fedichev, W. Zwerger, J. von Delft, and P. Zoller, *Phys. Rev. Lett.* **94**, 040404 (2005).
- [46] P. P. Orth, I. Stanic, and K. Le Hur, *Phys. Rev. A* **77**, 051601 (2008).
- [47] G. M. Falco, R. A. Duine, and H. T. C. Stoof, *Phys. Rev. Lett.* **92**, 140402 (2004).
- [48] E. Vernier, D. Pekker, M. W. Zwierlein, and E. Demler, *Phys. Rev. A* **83**, 033619 (2011).
- [49] A. V. Balatsky, I. Vekhter, and J.-X. Zhu, *Rev. Mod. Phys.* **78**, 373 (2006).
- [50] F. D. M. Haldane, *Phys. Rev. Lett.* **40**, 416 (1978).
- [51] J. R. Schrieffer and P. A. Wolff, *Phys. Rev.* **149**, 491 (1966).
- [52] P. W. Anderson, *J. Phys. C* **3**, 2435 (1970).
- [53] W. Hofstetter, *Phys. Rev. Lett.* **85**, 1508 (2000).
- [54] A. C. Hewson, J. Bauer, and W. Koller, *Phys. Rev. B* **73**, 045117 (2006).
- [55] J. Bauer and A. C. Hewson, *Phys. Rev. B* **76**, 035119 (2007).
- [56] This is justified by the local density approximation, which is usually a good description for trapped systems.
- [57] The energy resolution required is set by the peak width in Fig. 2 (b). For $n_{\text{imp}}/N_a \sim 0.1$ the width at $k = k_F$ is $\Delta/\varepsilon_F \sim 0.09$.